Engineering Analysis with Boundary Elements 11 (1993) 293–303

Boundary element analysis of anisotropic rock masses

B. Xiao & J.P. Carter

School of Civil and Mining Engineering, University of Sydney, New South Wales 2006, Australia

(Received 7 September 1992; revised version received 24 February 1993; accepted 2 March 1993)

A boundary element formulation is developed for anisotropic elastic rock masses. The boundary element treatment in which the fundamental solutions of Lekhnitskii have been incorporated, and the numerical evaluation of integrals with singularities are discussed. Good agreement found between the numerical and analytical solutions for several example problems demonstrates the capability, accuracy and efficiency of the present formulation. The problem of a deep circular tunnel excavated in a variety of jointed rock masses has also been analysed using the present formulation. The effect of the jointing on the behaviour of the rock mass around the tunnel is evaluated.

Key words: Boundary element method, elasticity, anisotropic, rock masses

1 INTRODUCTION

Natural rock masses are usually composed of blocks of intact material separated by joints or discontinuities. The behaviour of these rock masses is complex as it is governed not only by the properties of the intact rock but also by characteristics of the discontinuities. In general, the overall behaviour of a jointed rock mass will be anisotropic.

Most boundary element analyses carried out in geotechnical engineering assume that the rock mass can be modelled as an isotropic elastic material. There have been a few reported attempts to account for the structure of the rock mass in analyses, and examples of boundary element treatments of rock masses with distinct joints have been presented by Hocking[1] and Coulthard *et al.*[2] However, when the spacing between the joints is small in comparison with the length scale of interest (such as tunnel width or foundation size), a simulation incorporating the jointing explicitly is very difficult and costly to implement. The problem of dealing with the structure of the rock mass explicitly can be avoided in cases where the jointing is closely spaced and regular, because it is convenient in such problems to idealise the rock mass as an anisotropic elastic medium; that is, the effects of the discontinuities is implicit in the choice of the stress–strain model adopted for the equivalent rock mass continuum. Some of the boundary element treatments for anisotropic materials relevant to jointed rock masses are reviewed briefly below.

Rizzo and Shippy[3] and Crouch and Starfield[4] have assumed that in some cases rock masses may be represented as transversely anisotropic materials, and they have implemented into boundary element formulations the fundamental solutions due to Green[5] for a point force in an infinite sheet of transversely anisotropic elastic material. Brebbia[6] has also suggested an iterative-perturbation boundary element analysis for general anisotropic materials, and Dumir and Mehta[7] have analysed orthotropic half-plane problems using boundary element techniques using appropriate Airy stress functions. A boundary element formulation for general anisotropic materials has also been presented by Carter and Alehossein,[8] using the fundamental solutions derived by Lekhnitskii.[9]

This paper is an extension of the earlier work of Carter and Alehossein,[8] which made use of constant boundary elements to analyse anisotropic rock masses. In the present treatment, elements in which the displacements and tractions vary quadratically along the boundary have been adopted. The boundary element treatment incorporating the Lekhnitskii solutions for more general material anisotropy is presented. Because evaluation of singular integrals is an essential part of stress analysis with the boundary element method, schemes for the numerical computation of these integrals

Engineering Analysis with Boundary Elements 0955-7997/93/$06.00

are also presented. The capability, accuracy and efficiency of the boundary element formulation are verified by comparing the numerical solutions with independent analytical solutions for two example problems. To illustrate further the utility of the formulation, the problem of a deep circular tunnel excavated in rock masses containing a single set of joints is investigated in some detail.

2 ROCK MASS ANISOTROPY

For the purpose of analysis rock masses are often treated, at least as a first approximation, as linear, elastic, homogenous continua. However, it is well known that the mechanical properties of many rock masses depend on direction; i.e. they are anisotropic. The anisotropy is usually due to the presence of stratification, foliation or joints. Metamorphic rocks, rocks with distinct bedding, and rock masses cut by regular joint sets usually exhibit some degree of anisotropy.

A number of authors have described ways of incorporating the effects of planar elastic joints in the representation of a jointed rock mass as an anisotropic elastic continuum — e.g. Goodman and Duncan,[10] Goodman,[11] Carter and Alehossein,[8] and Xiao and Carter[12] — and so there is no need to repeat the derivation of the governing equations here. Instead, we proceed to a statement of the general compliance relations; i.e.

$$\begin{pmatrix} \epsilon_x \\ \epsilon_y \\ \epsilon_z \\ \gamma_{yz} \\ \gamma_{zx} \\ \gamma_{xy} \end{pmatrix} = \begin{bmatrix} c_{11} & c_{12} & \cdots & c_{16} \\ c_{12} & c_{22} & \cdots & c_{26} \\ \cdots & \cdots & \cdots & \cdots \\ c_{16} & c_{26} & \cdots & c_{66} \end{bmatrix} \begin{pmatrix} \sigma_x \\ \sigma_y \\ \sigma_z \\ \tau_{yz} \\ \tau_{zx} \\ \tau_{xy} \end{pmatrix} \tag{1}$$

or

$$\epsilon = C\sigma \tag{2}$$

where ϵ and σ are vectors of strain and stress components, respectively, and C is known as the compliance matrix. Specific forms of C have been considered elsewhere — e.g. Xiao and Carter.[12] Of particular interest is the case of an ideal rock mass where the intact material is isotropic and elastic, with a Young's modulus, E, and Poisson's ratio, v and the joints are planar, parallel and at a constant spacing, S. The elastic behaviour of each joint is characterised by uncoupled shear and normal stiffnesses, K_s and K_n. The specific case where the joints all strike parallel to the z-axis of a Cartesian coordinate system will be assumed later in this paper in the presentation of numerical solutions.

3 BOUNDARY ELEMENT FORMULATION

The anisotropic material behaviour described above can be incorporated in a boundary element solution procedure. The anisotropy is included via the fundamental solutions or Green's functions for the appropriate problem. In the following, attention is restricted to plane strain problems of anisotropy and in this case the Green's functions are for the problem of a line load embedded in the anisotropic medium.

If body forces are ignored, the direct formulation of the boundary element method leads to the following integral equation on the boundary of the two-dimensional body:

$$\alpha_{ij}(P)u_j(P) + \int_\Gamma T_{ij}(P,Q)u_j(Q)d\Gamma = \int_\Gamma U_{ij}(P,Q)t_j(Q)d\Gamma \tag{3}$$

where $\alpha_{ij}(P)$ is a constant which can be evaluated on the basis of rigid body displacements, as indicated by Watson,[13] Γ is the boundary of the element, and $u_j(Q)$ and $t_j(Q)$ are displacements and tractions in the j-coordinate direction at point Q on the boundary; $T_{ij}(P,Q)$ and $U_{ij}(P,Q)$ are fundamental solutions corresponding to the Kelvin problem of a line load buried in an infinite, general anisotropic elastic body.[9] Matrix $T_{ij}(P,Q)$ contains the fundamental solution for the boundary traction in the j-coordinate direction at point Q due to a load in the i-coordinate direction acting at a point P, and $U_{ij}(P,Q)$ contains the fundamental solution for the boundary displacements in the j-direction at point Q on the boundary due to a load in the i-direction at a point P. The fundamental solutions which have been derived by Lekhnitskii[9,14] are set out in Appendix 1 for completeness.

For a quadratic boundary element, the values of displacement and traction at any point on the element can be defined in terms of its nodal values and the interpolation functions, N_i; i.e.

$$t(\xi) = \sum_{i=1}^{3} N_i(\xi)t_i \tag{4}$$

$$u(\xi) = \sum_{i=1}^{3} N_i(\xi)u_i \tag{5}$$

where t_i, u_i are nodal values of tractions and displacements for the element and ξ is the local coordinate along the boundary. The geometry of the element can also be expressed as a quadratic function of the nodal coordinates; i.e.

$$x(\xi) = \sum_{i=1}^{3} N_i(\xi)x_i \tag{6}$$

$$y(\xi) = \sum_{i=1}^{3} N_i(\xi)y_i \tag{7}$$

where x_i, y_i are values of the coordinates of node i of the element. In this paper, the following forms are adopted for the interpolation functions $N_i(\xi)$, $N_2(\xi)$, $N_3(\xi)$:

$$N_1(\xi) = \tfrac{1}{2}(\xi - 1)\xi \tag{8}$$

$$N_2(\xi) = 1 - \xi^2 \tag{9}$$

$$N_3(\xi) = \tfrac{1}{2}(1 + \xi)\xi \tag{10}$$

If the field variables are approximated by eqns (4) and (5), then the discritised boundary integral equation can be written as

$$a_{ij}(P)u_j(P) + \sum_{k=1}^{M}\left\{\int_{\Gamma_k} T_{ij}(P,Q)N_k' d\Gamma\right\}\mathbf{u}_j(Q) = \sum_{k=1}^{M}\left\{\int_{\Gamma_k} U_{ij}(P,Q)N_k' d\Gamma\right\}\mathbf{t}_j(Q) \tag{11}$$

where M is the number of elements, Γ_k is the boundary of element k and $\mathbf{u}_j(Q)$ and $\mathbf{t}_j(Q)$ are now the nodal displacement and traction components of the element in the j-direction, respectively. N_k' is the matrix of interpolation functions for the element k; i.e.

$$N_k' = \begin{bmatrix} N_1(\xi) & 0 & N_2(\xi) & 0 & N_3(\xi) & 0 \\ 0 & N_1(\xi) & 0 & N_2(\xi) & 0 & N_3(\xi) \end{bmatrix} \tag{12}$$

Equation (11) can be written in matrix form for all the boundary points, so that

$$\boldsymbol{H}\mathbf{U} = \boldsymbol{G}\mathbf{P} \tag{13}$$

where $\boldsymbol{H}$ and $\boldsymbol{G}$ are matrices of influence coefficients, and vectors **U** and **P** contain the nodal displacements and tractions, respectively. Inserting the boundary conditions into eqn (13) allows the governing equations to be written as a set of linear simultaneous equations; i.e.

$$\boldsymbol{A}\mathbf{X} = \mathbf{F} \tag{14}$$

where the vector **X** contains all the boundary unknowns, **F** represents all the prescribed values of nodal traction or displacement and A is a matrix whose columns are a combination of columns of $\boldsymbol{H}$ and $\boldsymbol{G}$, according to the boundary conditions.

Once the set of equations (eqns (14)) has been solved and the values of displacements and tractions are known at all the nodes on the boundary, the displacements and stresses at any interior point can be determined by

$$u_i(P) = -\sum_{k=1}^{M}\left\{\int_{\Gamma_k} T_{ij}(P,Q)N_k' d\Gamma\right\}\mathbf{u}_j(Q) + \sum_{k=1}^{M}\left\{\int_{\Gamma_k} U_{ij}(P,Q)N_k' d\Gamma\right\}\mathbf{t}_j(Q) \tag{15}$$

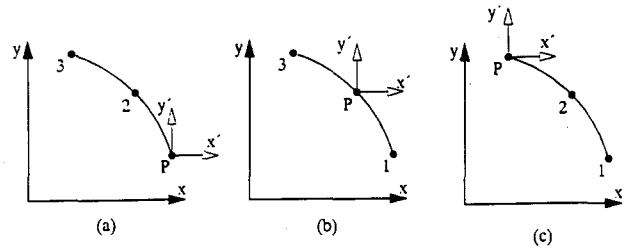

a b c

Fig. 1. The change of a global coordinate system to a local coordinate system; (a), (b) and (c) represent point P at nodes 1, 2 and 3.

$$\sigma_i(P) = \boldsymbol{D}\left[-\sum_{k=1}^{M}\left\{\int_{\Gamma_k} \boldsymbol{B}T_{ij}(P,Q)N_k' d\Gamma\right\}\boldsymbol{u}_j(Q) + \sum_{k=1}^{M}\left\{\int_{\Gamma_k} \boldsymbol{B}U_{ij}(P,Q)N_k' d\Gamma\right\}\mathbf{t}_j(Q)\right] \tag{16}$$

where $\boldsymbol{D}$ is the rigidity matrix, which is the inverse of matrix $\boldsymbol{C}$; i.e.

$$\boldsymbol{D} = \boldsymbol{C}^{-1} \tag{17}$$

$\boldsymbol{C}$ is the compliance matrix for plane strain problems in anisotropy, as described above. The matrix $\boldsymbol{B}$ appearing

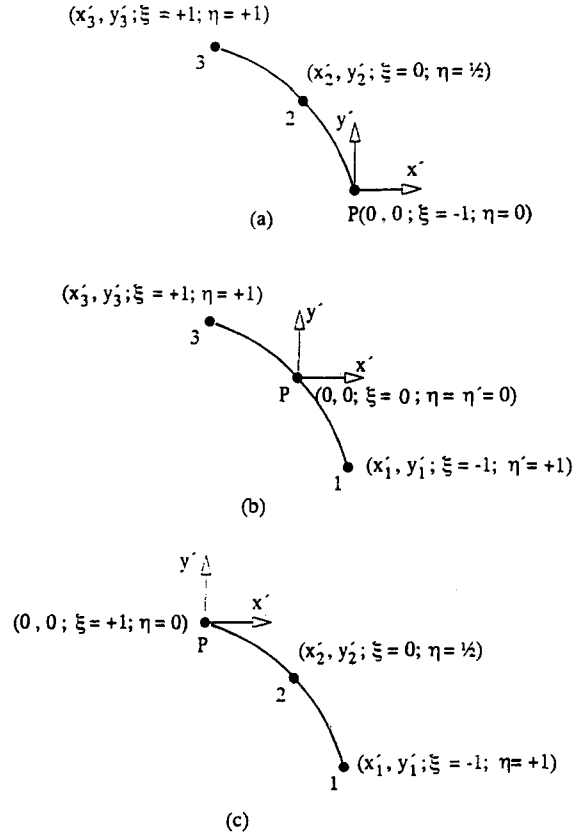

Fig. 2. Coordinate systems for numerical integration; (a), (b) and (c) represent point P at nodes 1, 2 and 3.

in eqn (16) is defined by

$$\boldsymbol{B} = \begin{bmatrix} \dfrac{\partial}{\partial x} & 0 \\ 0 & \dfrac{\partial}{\partial y} \\ \dfrac{\partial}{\partial y} & \dfrac{\partial}{\partial x} \end{bmatrix} \tag{18}$$

4 EVALUATION OF INTEGRALS CONTAINING A SINGULARITY

Some of the integrals in eqn (11) can be written in the form

$$\boldsymbol{I} = \int_{\Gamma_k} \ln (X + \rho_i Y) N_k' d\Gamma \tag{19}$$

where X, Y and ρ_i are defined in Appendix 1. If the point P is the same as the point Q, then both X and Y are identically zero and, obviously, the integrand becomes singular. Thus, care must be exercised if these integrals are to be evaluated accurately using numerical procedures. In this paper, the change of variable procedure is used for these numerical integrations. Three cases are considered, depending on whether point P is at node 1, 2 or 3 of the boundary element (see Figs 1 and 2).

4.1 Point P at node 1

Let (x_1, y_1), (x_2, y_2) and (x_3, y_3) represent the global coordinates of the nodes of a quadratic element k. The x, y global coordinate system is transformed to the x', y' coordinate system, as shown in Fig. 1(a), i.e.

$$x' = x - x_1 \tag{20}$$

$$y' = y - y_1 \tag{21}$$

A local coordinate ξ system is also defined along the boundary (Fig. 2). Using eqns (6) and (7), the terms X and Y in eqn (19) can be expressed as

$$X = \left(\frac{1+\xi}{2}\right)(A_{11}\xi + B_{11}) \tag{22}$$

$$Y = \left(\frac{1+\xi}{2}\right)(A_{12}\xi + B_{12}) \tag{23}$$

where the coefficients A_{11}, A_{12}, B_{11} and B_{12} are given in Appendix 2. Substituting eqns (22) and (23) into eqn (19) yields

$$\begin{aligned} \boldsymbol{I} = & \int_{-1}^{+1} \ln \left[\frac{1+\xi}{2}\right] N_k'(\xi) J(\xi) d\xi \\ & + \int_{-1}^{+1} \ln [(A_{11} + A_{12}\rho_i)\xi \\ & + (B_{11} + B_{12}\rho_i)] N_k'(\xi) J(\xi) d\xi \end{aligned} \tag{24}$$

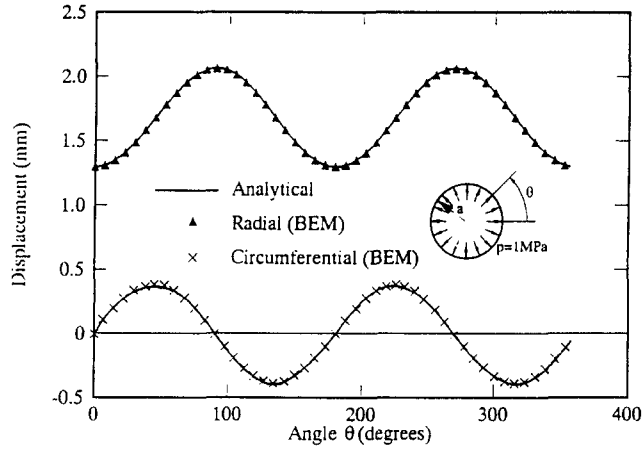

Fig. 3. Comparison of analytical and numerical solutions for displacements around the boundary.

where $J(\xi)$ is the Jacobian of the coordinate transformation. Here, the integral is divided into two parts, one with a singular term and the other with no singularity. In order to integrate the singularity, another change of variable from ξ to η is carried out (Fig. 2(a)) for the first integral. This transformation is defined as

$$\eta = \frac{\xi + 1}{2} \tag{25}$$

Equation (24) therefore becomes

$$\begin{aligned} \boldsymbol{I} = & 2\int_0^{+1} \ln \eta N_k'(\eta) J(\eta) d\eta \\ & + \int_{-1}^{+1} \ln [(A_{11} + A_{12}\rho_i)\xi \\ & + (B_{11} + B_{12}\rho_i)] N_k'(\xi) J(\xi) d\xi \end{aligned} \tag{26}$$

The first term in eqn (26) is integrated by means of the special integration formula suggested by Anderson.[15]

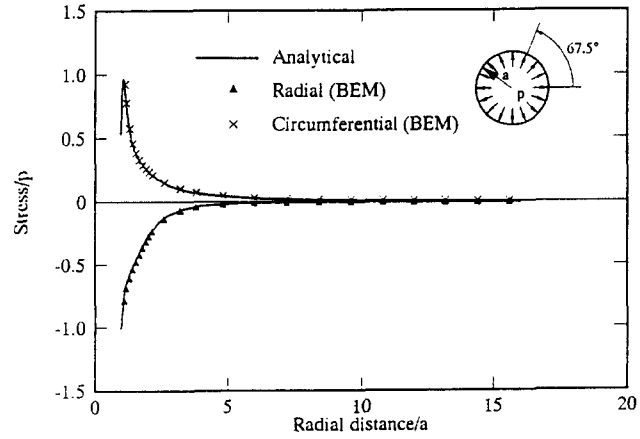

Fig. 4. Comparison of analytical and numerical solutions for stresses along a ray at 67·5° to the horizontal axis.

The second term is integrated by standard Gauss quadrature.

4.2 Point P at node 2

In this case, the change from the x, y global coordinate system to the x', y' coordinate system is carried out as shown in Fig. 1(b), and then a further transformation is made to the local coordinate ξ. Using eqns (6) and (7), the terms X and Y in eqn (19) can be expressed as

$$X = \xi(A_{21}\xi + B_{21}) \tag{27}$$

$$Y = \xi(A_{22}\xi + B_{22}) \tag{28}$$

where the coefficients A_{21}, A_{22}, B_{21} and B_{22} are given in Appendix 2. Substituting eqns (27) and (28) into eqn (19) and dividing it into two parts, with each part containing the singularity, gives

$$\begin{aligned} I = &\int_{-1}^{0} \ln[(-\xi)\{(A_{21} + A_{22}\rho_i)(-\xi) \\ &- (B_{12} + B_{22}\rho_i)\}]N_k'(\xi)J(\xi)d\xi \\ &+ \int_{0}^{+1} \ln[\xi\{(A_{21} + A_{22}\rho_i)\xi \\ &+ (B_{21} + B_{22}\rho_i)\}]N_k'(\xi)J(\xi)d\xi \end{aligned} \tag{29}$$

When ξ is replaced by $-\eta'$ and η in the first and second parts of eqn (29), then

$$\begin{aligned} I = &\int_{0}^{+1} \ln \eta' N_k'(\eta')J(\eta')d\eta' \\ &+ \int_{0}^{+1} \ln \eta N_k'(\eta)J(\eta)d\eta \\ &+ \int_{0}^{+1} \ln[(A_{21} + \rho_i A_{22})\eta' \\ &- (B_{21} + \rho_i B_{22})]N_k'(\eta')J(\eta')d\eta' \\ &+ \int_{0}^{+1} \ln[(A_{21} + \rho_i A_{22})\eta \\ &+ (B_{21} + \rho_i B_{22})]N_k'(\eta)J(\eta)d\eta \end{aligned} \tag{30}$$

The first and the second terms in eqn (30) are integrated by a special integration formula,[15] and the third and fourth terms are integrated by the Steffenson formula; i.e.

$$\begin{aligned} \int_0^1 f(x)dx \approx &\frac{11}{24}\left(f\left(\frac{1}{5}\right) + f\left(\frac{4}{5}\right)\right) \\ &+ \frac{1}{24}\left(f\left(\frac{2}{5}\right) + f\left(\frac{3}{5}\right)\right) \end{aligned} \tag{31}$$

4.3 Point P at node 3

This case is similar to the first case and terms X, Y in eqn (19) can be expressed as

$$X = \left(\frac{1-\xi}{2}\right)(A_{31}\xi + B_{31}) \tag{32}$$

$$Y = \left(\frac{1-\xi}{2}\right)(A_{32}\xi + B_{32}) \tag{33}$$

where the coefficients A_{31}, A_{32}, B_{31} and B_{32} are given in Appendix 2. Substituting eqns (32) and (33) into eqn (19) yields

$$\begin{aligned} I = &\int_{-1}^{+1} \ln\left(\frac{1-\xi}{2}\right)N_k'(\xi)J(\xi)d\xi \\ &+ \int_{-1}^{+1} \ln[(A_{31} + A_{32}\rho_i)\xi + (B_{31} + B_{32}\rho_i)] \\ &\times N_k'(\xi)J(\xi)d\xi \end{aligned} \tag{34}$$

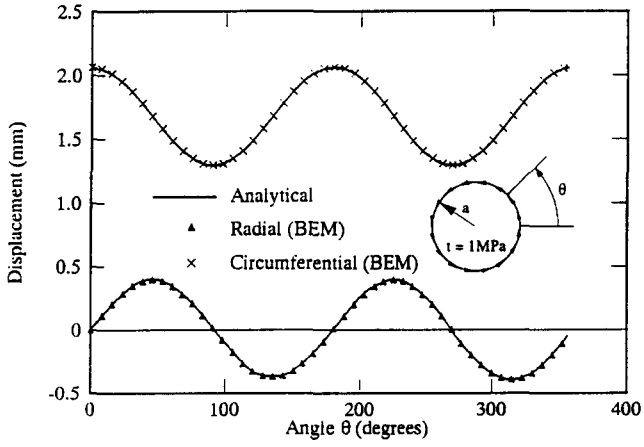

Fig. 5. Comparison of analytical and numerical solutions for displacements around the boundary.

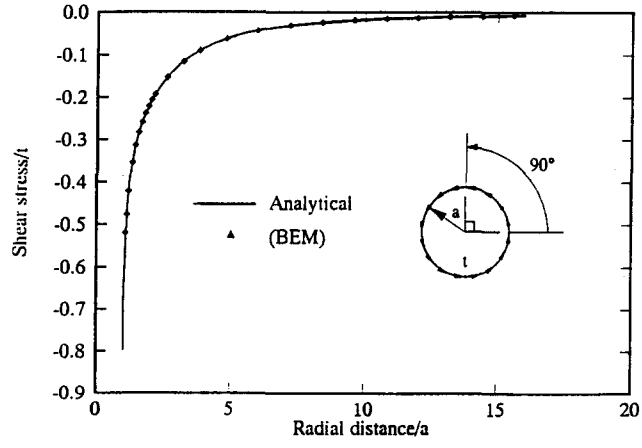

Fig. 6. Comparison of analytical and numerical solutions for shear stresses $\tau_{r\theta}$ along a ray at 90° to the horizontal axis.

Table 1. Comparison of accuracy of quadratic elements and constant elements (radial stresses along a line inclined at 22·5° to the x-axis)

Distance from boundary	Analytical solution σ_r (MPa)	24 quadratic elements σ_r (MPa)	Error %	24 constant elements σ_r (MPa)	Error %	48 constant elements σ_r (MPa)	Error %
$1{\cdot}5a$	−0·4996	−0·5010	0·28	−0·5117	2·36	−0·5064	1·34
$1{\cdot}8a$	−0·3576	−0·3576	< 0.1	−0·3771	5·17	−0·3632	1·54
$2{\cdot}5a$	−0·1042	−0·1042	< 0.1	−0·1111	6·21	−0·1066	2·25
$3a$	−0·0280	−0·0280	< 0.1	−0·0305	8·20	−0·0290	3·45
$5a$	0·0135	0·0135	< 0.1	0·0140	3.57	0·0136	0·74

A change of variable for the first part is defined by

$$\eta = \frac{1-\xi}{2} \tag{35}$$

Thus, eqn (34) may be written as

$$I = 2\int_0^{+1} \ln\ \eta N_k'(\eta)J(\eta)d\eta + \int_{-1}^{+1} \ln\ [(A_{31}+A_{32}\rho_i)\xi + (B_{31}+B_{32}\rho_i)] \times N_k'(\xi)J(\xi)d\xi \tag{36}$$

The first term in eqn (36) is integrated by means of the special integration formula.[15] The second term is integrated by standard Gauss quadrature.

5 VERIFICATIONS OF COMPUTER CODE

To validate the present formulation for anisotropic materials, problems involving normal pressure and shear tractions distributed uniformly over the surface of a cavity have been solved. The results have been compared with analytical solutions.[14]

The first problem concerns a circular cavity in an infinite anisotropic medium to which internal pressure ($p = 1$ MPa) is applied. The elastic compliance relations for this anisotropic body may be written as

$$\begin{bmatrix} \epsilon_x \\ \epsilon_y \\ \gamma_{xy} \end{bmatrix} = \begin{bmatrix} 0{\cdot}0833 & -0{\cdot}006 & 0 \\ -0{\cdot}006 & 0{\cdot}1667 & 0 \\ 0 & 0 & 1{\cdot}430 \end{bmatrix} \begin{bmatrix} \sigma_x \\ \sigma_y \\ \tau_{xy} \end{bmatrix} \tag{37}$$

where the compliance components in eqn (37) are in units of m^2/MN. Twenty-four quadratic boundary elements were used around the circular boundary; i.e. six in each quadrant. Figure 3 shows the predicted radial and circumferential displacements around the surface of the cavity. The distribution of radial and circumferential stresses along a radial line inclined at 67·5° to the horizontal (x-axis) are shown in Fig. 4. The numerical results agree very well with the analytical solution for this problem.

Consider also the case where there are shear tractions ($t = 1$ MPa) instead of normal pressure distributed uniformly over the surface of the cavity, and all other aspects of the problem are the same as in the previous example. For this case, the predicted displacements along the surface of the cavity and the shear stress $\tau_{r\theta}$ along a line inclined at 90° to the x-axis are shown in Figs 5 and 6, respectively. Very good agreement between the analytical and boundary element solutions is evident.

For the problem of normal pressure distributed uniformly over the surface of a cavity, Table 1 shows a comparison of radial stresses along a line inclined at 22·5° to the x-axis for selected points, using 24 quadratic elements, 24 constant elements and 48 constant elements. It is interesting to note that the use of quadratic elements gives more accurate results than constant elements, even when similar computing effort is required; for example, compare the results for 24 quadratic elements and 48 constant elements, both of which involve 48 nodes, and hence the solution of 96 equations.

6 ILLUSTRATIVE EXAMPLE

To illustrate further the utility of the formulation,

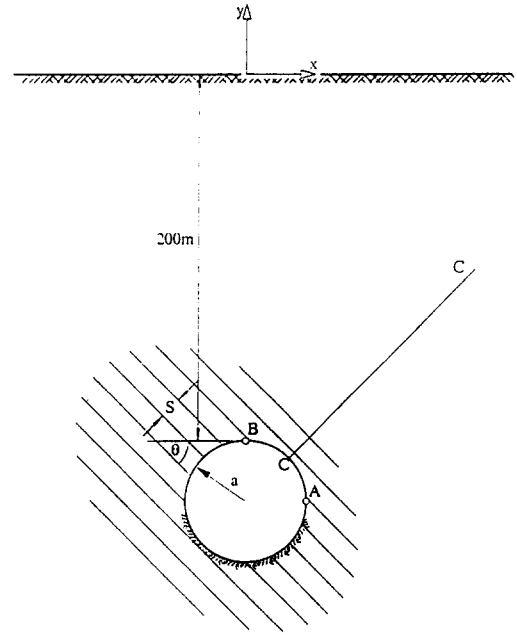

Fig. 7. Geometry of illustrative example.

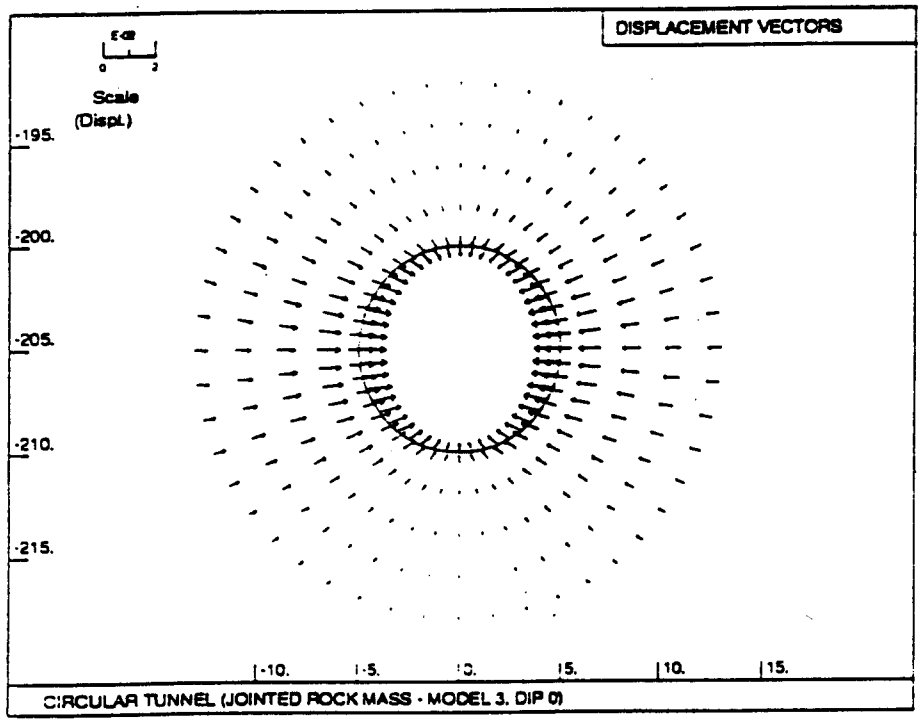

Fig. 8. The pattern of movement around the tunnel when the dip angle is 0°.

consider the following rock mechanics example. A circular tunnel is excavated in a jointed rock mass at a depth of 200 m below the surface (Fig. 7). The intact rock is characterised as an isotropic linearly elastic material and the anisotropy in the rock mass is introduced because of the presence of a single set of joints. The material properties of the rock mass are defined by

(a) Intact rock
Young's modulus, $E = 8000$ MPa
Poisson's ratio, $v = 0{\cdot}2$

(b) Joints
Normal stiffness, $K_n = 10\,000$ MPa/m
Shear stiffness, $K_s = 5000$ MPa/m

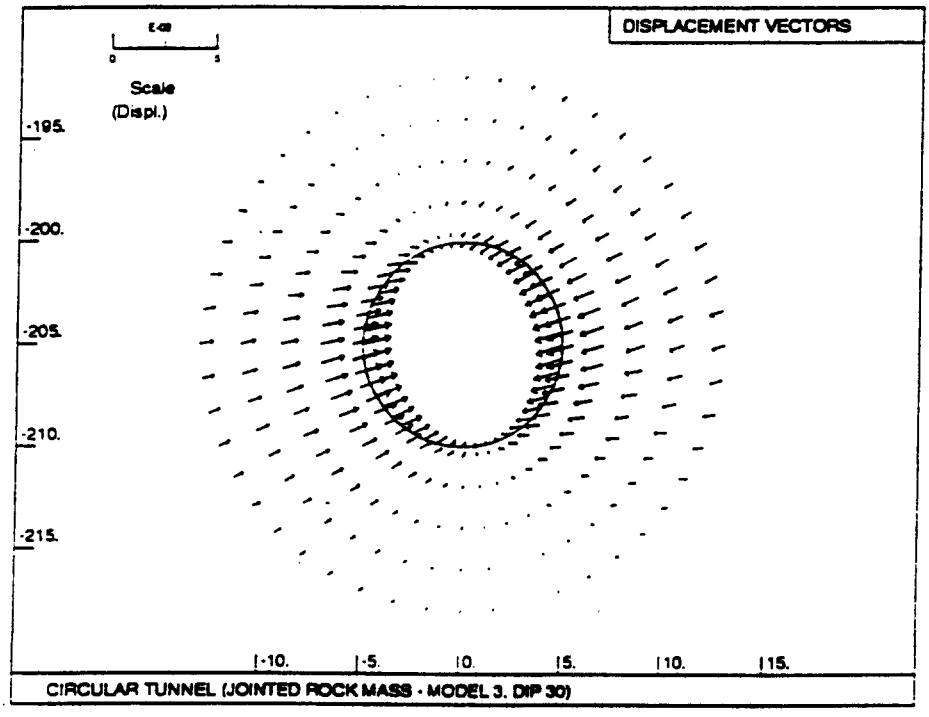

Fig. 9. The pattern of movement around the tunnel when the dip angle is 30°.

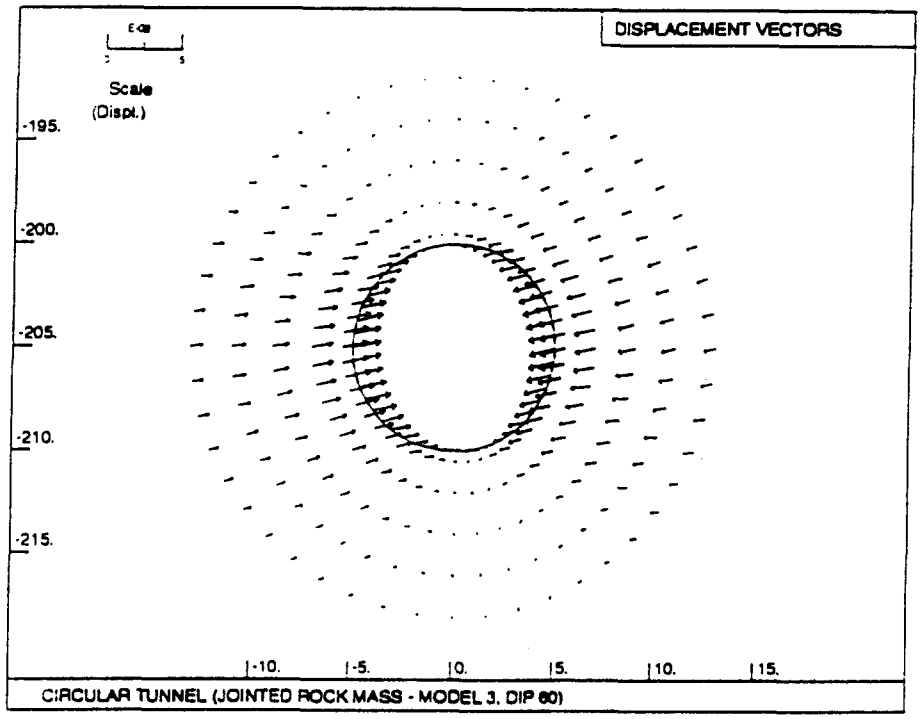

Fig. 10. The pattern of movement around the tunnel when the dip angle is 60°.

The in-situ vertical stress (prior to tunnelling) is assumed to vary with depth, according to

$$\sigma_v = \gamma d \tag{38}$$

where γ is the unit weight of the rock and d is the depth beneath the surface. The in-situ horizontal stress is

$$\sigma_h = K\sigma_v + q \tag{39}$$

where q is the surface value of the horizontal stress. The unit weight of the rock mass is assumed as $\gamma = 0.025\,\text{MN/m}^3$, the in-situ stress parameter $K = 2{\cdot}0$ and q is assumed equal to zero in this example. At a depth of 200 m the vertical and horizontal stresses are 5 MPa and 10 MPa, respectively. These average values are assumed to be the same over the full-depth interval of the tunnel.

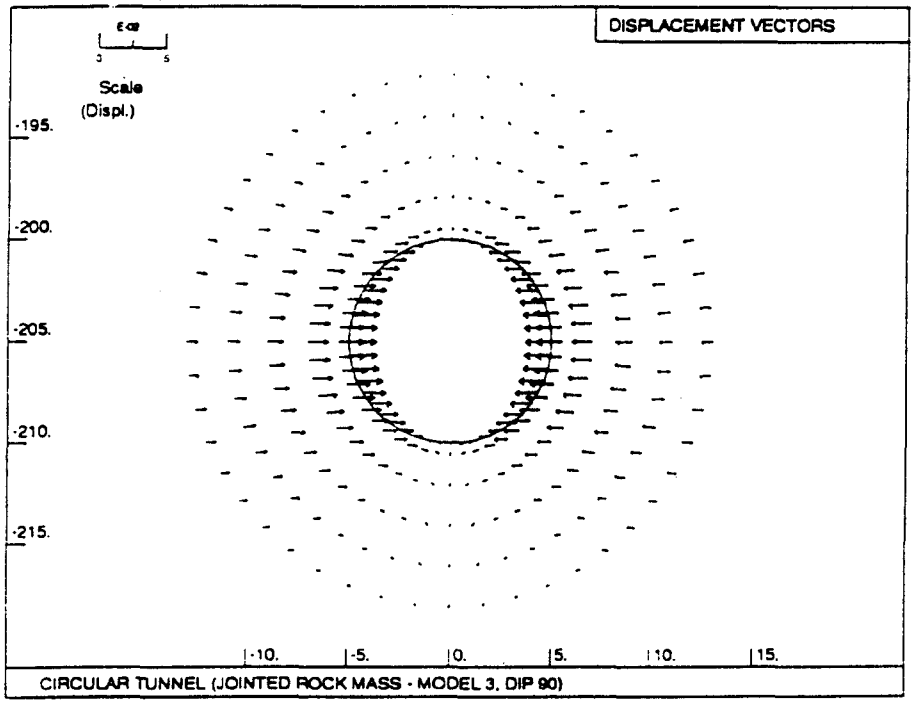

Fig. 11. The pattern of movement around the tunnel when the dip angle is 90°.

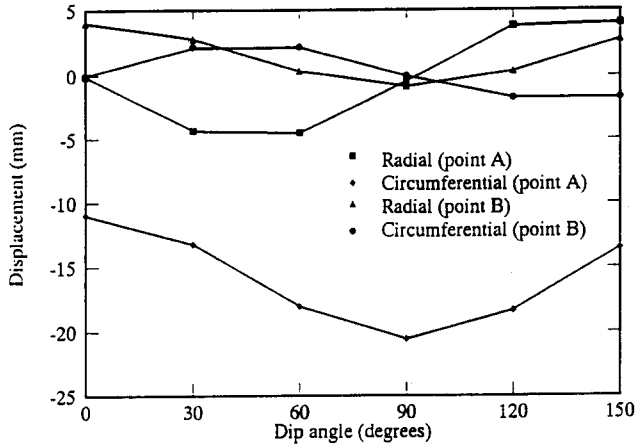

Fig. 12. Variations of displacements with the dip angle.

In each problem analysed, the joint set is assumed to strike parallel to the tunnel axis, i.e. perpendicular to the plane of the analysis, and initially the spacing of joints is assumed to be 1·0 m.

Figs 8–11 show the patterns of movement around the tunnel for dip angles of 0°, 30°, 60° and 90°, by indicating displacement vectors for selected points within the rock mass. The displacement distributions at boundary points *A* and *B* (Fig. 7) for dip angles ranging from 0 to 150 degrees are shown in Fig. 12. These figures show that the deformations around the tunnel are strongly affected by the inclination of the joints.

Cases where the joint set is assumed to strike parallel to the tunnel axis and the dip angle is 45° have also been analysed to examine the influence of the joint spacing on the rock mass behaviour. Three joint spacings (0·5, 1·0 and 1·5 m) have been considered and in each case the spacing is assumed constant throughout the rock mass. The predicted radial and circumferential displacements along line C–C (Fig. 7) have been plotted in Fig. 13. This figure shows that there is a decrease in the magnitude of the radial and circumferential displacements along line C–C as the spacing is increased, as might be expected.

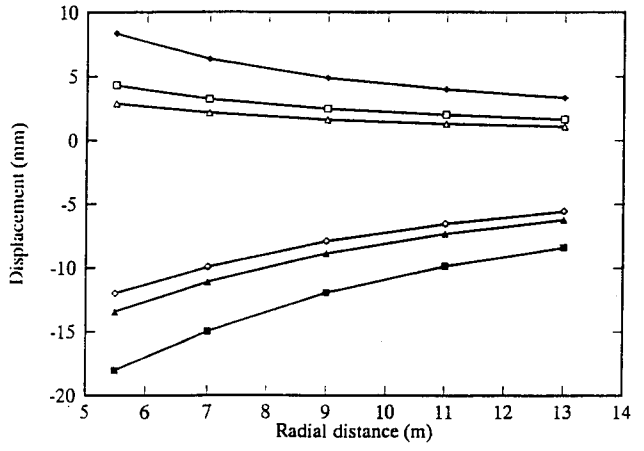

Fig. 13. Comparison of displacements along the C–C line. ■, Radial (0·5 m); ▲, radial (1·0 m); ◇, radial (1·5 m); ◆, circumferential (0·5 m); □, circumferential (1·0 m); △, circumferential (1·5 m).

7 CONCLUSIONS

The purpose of the present study was to develop an improved technique for the analysis of an anisotropic rock mass. The boundary element treatment in which Lekhnitskii's solutions have been incorporated, together with the evaluation of integrals containing a singularity, have been presented. The relative accuracy of constant and quadratic boundary elements has also been discussed. Example problems have been solved to demonstrate the capability, accuracy and efficiency of the present formulation. Moreover, the results of one of the examples show that the orientation and spacing of the joint sets have a considerable influence on the behaviour of a rock mass around a tunnel.

One of the attractions of the boundary element formulation presented here is that it may be easily coupled with a finite element procedure, particularly as quadratic boundary elements have been employed. A coupled boundary element–finite element formulation could then be used to analyse problems involving nonlinear and anisotropic rock mass behaviour. The coupled analysis will be the subject of a future paper.

ACKNOWLEDGEMENTS

The work described in this paper forms part of an ongoing study into the behaviour of deep excavations in urban environments, which is supported by a grant from the Australian Research Council. Support for this work is also provided in the form of a research scholarships awarded to B.X. by the Australian Development Cooperation Scholarship Scheme and by the Centre for Geotechnical Research at the University of Sydney.

REFERENCES

1. Hocking, G.A. Stress analysis of underground excavations incorporating slip and separation along discontinuities, *Recent Advances in the Boundary Element Method,* Pentech Press, 1978, pp. 195–214.
2. Coulthard, M.A., Crotty, J.M. & Fabjanceyk, M.W. Comparison of field measurements and numerical analyses of a major fault in a mine pillar. *Proc. 5th Int. Cong. on Rock Mech., ISRM,* Melbourne, Balkema, Rotterdam, 1983, Vol. 4, pp. 53–60.
3. Rizzo, F.J. & Shippy, D.J. A method for stress determination in plane anisotropic elastic bodies. *J. Comp. Mat.,* 1970, **4,** 36–60.
4. Crouch, S.L. & Starfield, A.M. *Boundary Element Methods in Solid Mechanics,* George Allen and Unwin, London, 322pp.
5. Green, A.E. A note on stress systems in aeolotropic materials, *Phil. Mag.,* 1943, **34,** 416–18.

6. Brebbia, C.A. *The Boundary Element Method for Engineers*, 2nd edn, Pentech, 1980, pp. 174–6.
7. Dumir, P.C. & Mehta, A.K. Boundary element solution for elastic orthotropic half-plane problems. *Comp. Struct.*, 1987, **26**, 431–8.
8. Carter, J.P. & Alehossein, H. Analysis of tunnel distortion due to an open excavation in jointed rock, *Comp. Geotech.*, 1990, **9**, 209–31.
9. Lekhnitskii, S.G. Plane static problem of the theory of elasticity of an anisotropic body, *Prikl. Mat. i Mekh., Nov. Seriya*, 1937, **I** (1).
10. Goodman, R.E. & Duncan, J.M. The role of structure and solid mechanics in the design of surface and underground excavations in rock. *Structure Solid Mechanics and Design, Proc. Civil. Eng. Material Conf. (2)*, ed. M. Terini, Southampton, 1969.
11. Goodman, R.E. *Introduction to Rock Mechanics*, John Wiley & Sons, New York, 1980, 478 pp.
12. Xiao, B. & Carter, J.P. Boundary element analysis of anisotropic rock masses, Research Report, No. R657, School of Civil and Mining Engineering, University of Sydney, Australia, 1992.
13. Watson, J.O. Advanced implementation of the boundary element method for two- and three-dimensional elastostatics, *Developments in Boundary Element Methods — 1*, ed. P.K. Banerjee and R. Butterfield, Applied Science Publishers, London, 1979, pp. 31–61.
14. Lekhnitskii, S.G. *Theory of Elasticity of an Anisotropic Body*, Mir, Moscow, 1981, 430 pp.
15. Anderson, D.G. Gaussian quadrature formulae for $\int_0^1 -\ln(x) f(x)dx$. *Math. Comp.*, 1965, **19**, 477–81.

APPENDIX 1: FUNDAMENTAL SOLUTIONS FOR PROBLEMS IN PLANE ANISOTROPY

The Lekhnitskii solutions[9,14] for a line load in an infinite anisotropic medium may be expressed as follows.

With reference to Fig. A1.1 the displacement components (u, v) and the stress components $(\sigma_x, \sigma_y, \tau_{xy})$ at Q due to unit line loads at P acting in the coordinate directions may be written in the form

$$\mathbf{U}(x,y) = \begin{pmatrix} u \\ v \end{pmatrix} = 2\mathrm{Re}\begin{bmatrix} a_1A_1\ln Z_1 + b_1B_1\ln Z_2 & a_2A_1\ln Z_1 + b_2B_1\ln Z_2 \\ a_1A_2\ln Z_1 + b_1B_2\ln Z_2 & a_2A_2\ln Z_1 + b_2B_2\ln Z_2 \end{bmatrix} \tag{A1.1}$$

and

$$\mathbf{S}(x,y) = \begin{pmatrix} \sigma_x \\ \sigma_y \\ \tau_{xy} \end{pmatrix} = 2\mathrm{Re}\begin{bmatrix} \rho_1^2A_1\left(\frac{1}{Z_1}\right) + \rho_2^2B_1\left(\frac{1}{Z_2}\right) & \rho_1^2A_2\left(\frac{1}{Z_1}\right) + \rho_2^2B_2\left(\frac{1}{Z_2}\right) \\ A_1\left(\frac{1}{Z_1}\right) + B_1\left(\frac{1}{Z_2}\right) & A_2\left(\frac{1}{Z_1}\right) + B_2\left(\frac{1}{Z_2}\right) \\ -\rho_1A_1\left(\frac{1}{Z_1}\right) - \rho_2B_1\left(\frac{1}{Z_2}\right) & -\rho_1A_2\left(\frac{1}{Z_1}\right) - \rho_2B_2\left(\frac{1}{Z_2}\right) \end{bmatrix} \tag{A1.2}$$

where Re indicates the real part of the components between square brackets. The parameters Z_1 and Z_2 are defined by

$$Z_1 = X + \rho_1 Y \tag{A1.3}$$

$$Z_2 = X + \rho_2 Y \tag{A1.4}$$

where X and Y are the Cartesian components of the distance between the point P and the point Q, as shown in Figure A1.1. Complex numbers ρ_1 and ρ_2 and their conjugates are the roots of

$$c_{11}\rho^4 - 2c_{13}\rho^3 + (2c_{12} + c_{33})\rho^2 - 2c_{23}\rho + c_{22} = 0 \tag{A1.5}$$

where c_{ij} are the components of the 3×3 symmetric compliance matrix C for plane strain problems.

Parameters a_1, a_2, b_1 and b_2 in eqn (A1.1) are given by

$$a_1 = c_{11}\rho_1^2 + c_{12} - c_{13}\rho_1 \tag{A1.6}$$

$$a_2 = c_{12}\rho_1 + \frac{c_{22}}{\rho_1} - c_{23} \tag{A1.7}$$

$$b_1 = c_{11}\rho_2^2 + c_{12} - c_{13}\rho_2 \tag{A1.8}$$

$$b_2 = c_{12}\rho_2 + \frac{c_{22}}{\rho_2} - c_{23} \tag{A1.9}$$

The complex coefficients A_1, B_1, and A_2, and B_2 in eqns (A1.1) and (A1.2) are obtained from the solution of two sets of simultaneous equations with complex coefficients, i.e.

$$\begin{bmatrix} 1 & 1 & -1 & -1 \\ \rho_1 & \rho_2 & -\bar{\rho}_1 & -\bar{\rho}_2 \\ \rho_1^2 & \rho_2^2 & -\bar{\rho}_1^2 & -\bar{\rho}_2^2 \\ \frac{1}{\rho_1} & \frac{1}{\rho_2} & -\frac{1}{\bar{\rho}_1} & -\frac{1}{\bar{\rho}_2} \end{bmatrix} \begin{bmatrix} A_1 \\ B_1 \\ \bar{A}_1 \\ \bar{B}_1 \end{bmatrix} = \frac{1}{2\pi i} \begin{bmatrix} 0 \\ -1 \\ -\frac{c_{13}}{c_{11}} \\ \frac{c_{12}}{c_{22}} \end{bmatrix} \tag{A1.10}$$

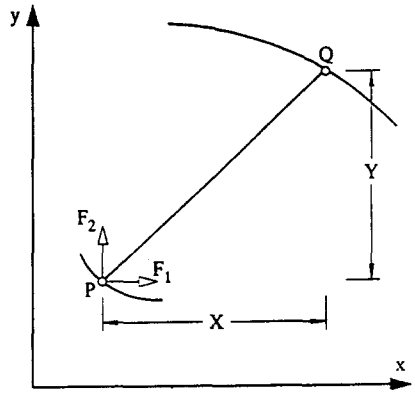

Fig. A1.1. Line loads in an infinite anisotropic medium.

and

$$\begin{bmatrix} 1 & 1 & -1 & -1 \\ \rho_1 & \rho_2 & -\bar{\rho}_1 & -\bar{\rho}_2 \\ \rho_1^2 & \rho_2^2 & -\bar{\rho}_1^2 & -\bar{\rho}_2^2 \\ \frac{1}{\rho_1} & \frac{1}{\rho_2} & -\frac{1}{\bar{\rho}_1} & -\frac{1}{\bar{\rho}_2} \end{bmatrix} \begin{bmatrix} A_2 \\ B_2 \\ \bar{A}_2 \\ \bar{B}_2 \end{bmatrix} = \frac{1}{2\pi i} \begin{bmatrix} 1 \\ -0 \\ -\frac{c_{12}}{c_{11}} \\ \frac{c_{23}}{c_{22}} \end{bmatrix} \tag{A1.11}$$

The Green's functions for displacement required in a plane strain boundary element analysis can be obtained from the coordinate components of displacement given in eqn (A1.1). The Green's functions for the tractions can be obtained simply from the stress components defined in eqn (A1.2).

APPENDIX 2: DETAILS OF COORDINATE TRANSFORMATIONS

The coefficients A_{ij} and B_{ij} $(i = 1,2,3;\ j = 1,2)$ in eqns (22), (23), (27), (28), (32) and (33) are given in the global x, y coordinate system as follows:

$$A_{11} = x_1 - 2x_2 + x_3 \tag{A2.1}$$

$$B_{11} = 2(x_2 - x_1) \tag{A2.2}$$

$$A_{12} = y_1 - 2y_2 + y_3 \tag{A2.3}$$

$$B_{12} = 2(y_2 - y_1) \tag{A2.4}$$

$$A_{21} = (x_1 - 2x_2 + x_3)/2 \tag{A2.5}$$

$$B_{21} = (x_3 - x_1)/2 \tag{A2.6}$$

$$A_{22} = (y_1 - 2y_2 + y_3)/2 \tag{A2.7}$$

$$B_{22} = (y_3 - y_1)/2 \tag{A2.8}$$

$$A_{31} = -(x_1 - 2x_2 + x_3) \tag{A2.9}$$

$$B_{31} = 2(x_2 - x_3) \tag{A2.10}$$

$$A_{32} = -(y_1 - 2y_2 + y_3) \tag{A2.11}$$

$$B_{32} = 2(y_2 - y_3) \tag{A2.12}$$